A New Lagrangian–Eulerian Coupling Model System

Rudklao Manonom

Business Management Department, Electricity Generating Authority of Thailand, 53 Charan Sanit Wong Road, Bang Krui, Nonthaburi 11130, Thailand

Lei Xiaoen (雷孝恩)

LAPC, Institute of Atmospheric Physics (IAP), Chinese Academy of Sciences, Beijing 100029

Prungchan Wongwises

King Mongkut's University of Technology Thonburi, 91 Pracha-Utit Road, Bangmod, Thongkru, Bangkok 10140, Thailand

(Received December 22, 1999; revised January 21, 2000)

ABSTRACT

A new Lagrangian–Eulerian coupling model system is developed to study regional air quality. The system consists of mesoscale dynamical meteorological model (MM), Monte-Carlo model (MCM), parameterized model on planetary boundary layer (PBL) turbulent statistics, dry and wet removal model, and Eulerian nonlinear chemical model (ENCM). The physical, chemical and biological processes on air pollutants are considered comprehensively. 3-D distribution laws for acidic gaseous pollutants (SO_2 and NO_x) emitted by Thai Mae Moh Power Plant and the secondary pollutants are studied in detail. The results simulated by the coupling model system are in good agreement with observational concentration data.

Key words: MM, MCM, ENCM, Coupling model system

1. Introduction

Studies of the physical, chemical and biological processes on air pollutants in turbulent flow have been developed along two main lines which are Lagrangian frame of reference and Eulerian gradient transfer theory. Both the theories are all to solve a set of species conservation equations (Lei, Han, and Zhang, 1998).

The starting of the Lagrangian theory is to integrate the following species conservation equation:

$$< \chi_i(r,t) > = \int_0^t \int_0^r p_r(r,t|r't')S_i(r't')dr'dt', \tag{1}$$

where subscript i represents different species, r and r' denote particle locations at time t and t', χ, p_r and S are species (or particle) concentration, probability density function, and source (or sink) function, respectively.

Several important features of the Lagrangian approach are that: 1) It can represent well the randomness of the atmospheric turbulence. 2) The approach is basic simplicity in concept and application. 3) The theory is free of the closure problem that handicaps the Eulerian theory. 4) There is no the restricting assumption that the length scale of the spatial variation on species must be much larger than the advective length scale of the turbulent eddy in the

gradient transfer theory. 5) There is no difficulty in numerical calculation (such as the numerical diffusion problem) compared with solving the partial differential equation. 6) The MCM can explicitly account for effects on calm wind, wake turbulence, and temporal and spatial variations of atmospheric condition or source emission.

The two main weaknesses of the Lagrangian theory are that it is applicable only to linearly reactive species and Lagrangian parameters cannot be directly measured. Both of them are just the chief advantages of the Eulerian theory.

In order to overcome the weaknesses of the Lagrangian model, a new Lagrangian–Eulerian coupling model will be developed to study regional distributions of acidic gaseous pollutants (SO_2 and NO_x) emitted by the Thai Mae Moh Power Plant and the secondary pollutants.

2. Overview of coupling model system

2.1 *Mesoscale dynamical meteorological model*

In order to support emergency response on air pollution and simulate regional air quality, the MCM requires inputting hourly 3–D horizontal wind fields, temperature, and rainfall rate over the model domain. The MM (Anthe, 1987; Guo, 1994; Dudhia, 1996) is currently used to generate these data.

2.1.1 *Governing equations*

The MM is a 3–D, limited–area, hydrostatic, primitive equation model written in a terrain–following z^* coordinate,

$$z^* = z_H(z - z_g)/(z_H - z_g), \tag{2}$$

where z_g is local topography height as a function of x and y, z_H is height of the model top and it is a constant. The top of the model domain is exactly flat and the bottom follows the terrain (Walko, 1995; McQueen, 1996).

The governing equations consist of motion, thermodynamic, and continuity equation. Many surface variables such as landuses, terrain height, roughness length $z_0(x,y)$, and ground temperature are ingested into the model grid.

2.1.2 *Numerical algorithms*

The horizontal grid structure is "staggered", with momentum variables defined at one set of grid points and all other variables defined at the offset points. In order to increase resolution near the surface layer, the variable vertical grid spacing is used. The vertical velocity is defined at boundaries between the layers, while all other variables are calculated at middle of the layers.

To solve the governing equations, the staggered difference scheme is used. The finite difference equations are written with the Donor scheme for advective terms.

The leapfrog scheme is used for the time difference scheme. In order to prevent splitting of the solutions often associated with the leapfrog scheme and reduce the amount of energy in waves with high frequency, the following frequency filter is applied to all prognostic variables,

$$<\alpha>^{\tau} = (1-v)\alpha^{\tau} + 0.5v(\alpha^{\tau+1} + <\alpha>^{\tau-1}), \tag{3}$$

where α is a filtered variable, and the coefficient $v = 0.1$.

2.1.3 *Initial and boundary conditions*

The initial fields of wind and temperature are created by a diagnostic model. It consists of three parts which are continuity equation, adjustment of meteorological field, and objective interpolation of measured data.

For the lower boundary conditions, the surface layer fluxes provide the main exchange of information between the atmosphere and the surface. It is convenient for numerical reasons to define variable values at a fictitious $0.5\Delta z^*$ under the surface. The variable values at the surface are specified by the objective interpolation of measured data.

The absorbing boundary condition at the model top can be determined by the following expression:

$$< F_{ijk} > = F_{ijk} - r(F_{ijk} - F_{ijN}),$$

where F is any variable, $r = 1.0, 0.75, 0.5$, and 0.25 at layer $k = N-3, \cdots, N$, respectively.

The inflow and outflow lateral boundary conditions are used. The variable values at the lateral boundaries are specified by the objective interpolation of observational data.

2.1.4 *Four-dimensional data assimilation(FDDA)*

A "nudging" type of the FDDA scheme has been implemented in the MM, in which the model fields can be nudged toward observational data.

The general form for predictive equation of any variable, A, is written as

$$\partial A / \partial t = F + G_\alpha (A_0 - A). \tag{5}$$

All of the model's physical forcing terms are represented by F. The second term on the right hand side of (5) is the nudging term, where G_α is a positive nudging factor (Seaman, 1989; Stauffer, 1990). $G_\alpha = 5 \times 10^{-3}$ is appropriate for the Thai Mae Moh area.

2.2 *Monte-Carlo model*

The MCM involves writing an equation for the random fluctuation velocity of a particle and then constructing trajectories of thousands of individual particles. At certain times or distances downstream, the resulted concentration distribution can be obtained.

2.2.1 *Particle trajectory*

The equation for the total particle velocity in direction "i" (Lei and Deng, 1988) is

$$u_i = U_i + u_i'(t)\rho_L{}^i(\Delta t) + \rho_i, \tag{6}$$

where U_i is given by the MM output, and u_i' is the turbulent component. The second term on the right hand side of (6) is the correlated component and the third term is the random component. $\rho_L{}^i$ is the Lagrangian auto-correlation coefficient for component "i" and time step Δt. $i = 1, 2, 3$ represents u, v, w^* components of velocity, respectively. ρ_i is the Monte-Carlo component which is picked randomly from a Gaussian distribution with zero mean and standard deviation $\sigma_{\rho i}$ given by the formula

$$\sigma_{\rho i} = \sigma_i \{1 - [\rho_L{}^i(\Delta t)]^2\}^{1/2}, \tag{7}$$

where σ_i is the standard deviation of the local turbulent fluctuation. An exponential form for $\rho_L{}^i$ is assumed

$$\rho_L{}^i(\Delta t)= \exp(-\Delta t / T_L{}^i), \tag{8}$$

where $T_L{}^i$ is the Langrangian time scale.

Considering particles which undergo a series of displacements are composed of three distinct components. The total trajectory for the particle is given by

$$x_{\alpha i} = x_{0\alpha i} + \sum_{n=1}^{N_0} u_{n\alpha i}\Delta t, \tag{9}$$

where N_0 is the tracked step number, α is the label for emitted particles.

2.2.2 *Species concentration*

The expression for the concentration distribution from a continuous source can be written as

$$\chi(r,t)= p_r Q \Delta t_0, \tag{10}$$

where Δt_0 is the time interval emitted instantaneous source, Q is the emission rate of particles from a source located at r_s. p_r can be obtained by the following formula:

$$p_r(r,t)= \sum_{n=1}^{M_0} p_{rq}(r,t)/ M_0, \tag{11}$$

where p_{rq} is the probability density for an instantaneous source, and M_0 is the total number of instantaneous sources for approximating each continuous source.

The p_{rq} is reduced by the following expression

$$p_{rq}(r,t)= \sum_{\alpha=1}^{N_0} \delta[r- r_\alpha(t,t_{0\alpha})]/ [M_0 \Delta x_r \Delta y_r \Delta z_r^*], \tag{12}$$

where Δx_r, Δy_r, Δz_r^* is a volume element, $t_{0\alpha}$ is the time leaving source for labelled particle α.

2.3 *Parameterized model on PBL turbulent statistics*

The MCM is not directly related to turbulent fluctuation, mostly the relation is fitted by its statistics. Standard deviations of the turbulent fluctuation (σ_u, σ_v, σ_w), Lagrangian time scales ($T_L{}^u$, $T_L{}^v$, $T_L{}^w$), and velocity scales (u_* and w_*) are most important PBL turbulent statistics to study turbulent diffusion (Hanna, 1979; Stull, 1988). They are also basic parameters inputting into the MCM. The parameterized model of variations on these statistics with height, z_0 and atmospheric stability in the PBL was developed by Lei (1988).

2.4 *Dry and wet removal model*

Correct parameterizations of dry and wet deposition processes are very important for understanding the evolution law of trace gases in the regional scale range.

2.4.1 *Dry deposition process*

The change rate of selected species due to dry deposition is commonly modelled in term of dry deposition velocity (V_d) and the expression can be written as

$$d\chi / dt = - V_d d\chi / dz \approx - V_d \chi / z_1, \tag{13}$$

where z_1 is height of the lowest model layer. After integrating (13) and using $\chi_d = \chi(t)$, $\chi_a = \chi(0)$, we obtain

$$\chi_d = \chi_a \exp(-V_d t / z_1). \tag{14}$$

where χ_d and χ_a are concentrations of species with and without effect of V_d, respectively.

2.4.2 *A new dry deposition velocity pattern(NDDVP)*

Lei (1996) developed an NDDVP to study the dry deposition processes. The following expression of the new V_d had been obtained

$$V_d = 79.5[(z_1 - z_d)r_c^{-1.46} / (r_a + r_b)]^{1/2} \quad (\mathrm{cm/s}). \tag{15}$$

where z_1 and z_d are the reference height and the mass sink height respectively, and

$$r_b = \ln(z_0 / z_d) / (0.36u_*), \tag{16}$$

$$r_a = \int_{z_0}^{z_d} dz / K_z. \tag{17}$$

where r_c is the total resistance in the plant canopy layer or at the ground level, K_z is the eddy diffusion along the z^* direction.

2.4.3 *Wet deposition process*

We can obtain the following expression similar to that of the dry deposition process.

$$\chi_w = \chi_a \exp(-\lambda t). \tag{18}$$

where λ is the scavenging coefficient, which depends on gaseous species, rainfall rate, and landuses. χ_w is the concentration taking account of rain process effect (Scott, 1982; Lei, Jia and Yuan, 1987).

2.5 *Eulerian nonlinear chemical model*

The gas phase chemistry (18 chemical reactions for 11 chemical species) consists of photochemical reaction, thermal reaction, Troe reaction, equilibrium reaction, and special reaction in the ENCM. The inorganic chemistry is only considered.

The chemical rate equations are integrated using a two-step method which exploits the exponential solution to the generic differential equation of chemical kinetics (NAPAP, 1990; Lei and Chang, 1992).

$$\partial\chi_j / \partial t = P_c(\chi_i) - [\chi_j / L_c(\chi_i)]. \tag{19}$$

where χ_i is the value of the j-th species, $P_c(\chi_i)$ and $L_c(\chi_i)$ are the production rate and characteristic loss time scale, both of which explicitly depend on χ_i. A lot of complex nonlinear chemical reactions are included in Equation (19).

There are three cases for all species. If $\partial\chi_j / \partial t = 0$, then $\chi_j = P_c(\chi_i) / L_c(\chi_i)$; HO_2, HO, ground state oxygen atom (O^3p), and excited state oxygen atom(O^1D) belong to this kind: the species concentrations are obtained by iteratively solving an implicit set of steady state equations. If $L_c(\chi_i) = 0$ and $\partial\chi_j / \partial t = P_c(\chi_i)$, then $\chi_j^{t+\Delta t} = P_c(\chi_i)\Delta t + \chi_j^t$; SO_4^{2-} belongs to this kind. If P_c and L_c are constants during a Δt, the solution to (19) is

$$\chi(t + \Delta t) = P_c \times L_c + [\chi(t) - P_c \times L_c]\exp(\Delta t / L_c). \tag{20}$$

where $\chi(t+\Delta t)$ is the value at $t+\Delta t$.

2.6 *Lagrangian MCM coupling with ENCM*

The Lagrangian MCM coupling with ENCM is made in the following order: First, all emitted particle trajectories are tracked by the Lagrangian MCM. Second, the transport and diffusion processes of the particles are calculated. Third, 3–D particle distributions are memorized in a particle file, they will be used as initial particle distributions at next time step. Fourth, the particles are converted to Eulerian concentration fields. Fifth, dry and wet deposition processes are calculated. Sixth, the nonlinear chemical processes are simulated by the ENCM. Seventh, 3–D concentration distributions for all species are memorized in a concentration file, they will be used as initial concentration distributions at next time step. Eighth, program loop goes back to the first step and the integral of next time step is started.

For every time loop, the transport, diffusion, dry and wet removal processes on air pollutants are simulated with the Lagrangian MCM, the chemical transformation processes for all species are calculated only by the ENCM.

3. Test of model system

3.1 *Selection of practical cases*

The Mae Moh Power Plant is situated in the northern Thailand. It generates about 30% of Thai electricity. The modeling domain covers an area 94×94 km^2 around the power plant. From the isohypse distribution in Fig.1 we can see that the terrain is very complex in the model area. The height difference between the lowest elevation and the mountain peak is about 300–1000 m. Owing to the effect of violent downdraft on the leeward side of the mountain range, and huge rising and fallings of terrain, the flow pattern in the surface boundary layer is obviously different from the plain at the same latitude.

There are 8 landuses in the model domain. They are urban land, agriculture, range, forest, water, swamp, mixing agriculture and range, and rocky open area with low–growing shrub.

The coupling model system is subdivided over the study area into 13 levels extending up to 2 km (Table 1) in the vertical. The computing mesh interval is $\Delta x=\Delta y=2$ km in the horizontal.

Table 1. Vertical layer of the model

K	1	2	3	4	5	6	7	8	9	10	11	12	13
z($\times10$ m)	0.5	1	2.5	5	7.5	10	20	40	60	80	100	150	200

Six typical cases in February and March 1996 are selected and good data on monitoring networks can be used. Different weather conditions have been included in the six cases.

3.2 *Data inputting into model system*

The following basic data must be input into the model system: emission inventory of source; ground temperature and radiation; geography elevation; species concentration; parameters of the near surface layer; rainfall amount; and 3–D wind and temperature fields.

There are ten surface weather stations, two upper–air stations, and one Doppler sodar observational station in the model area. A set of surface and upper–air data can be obtained

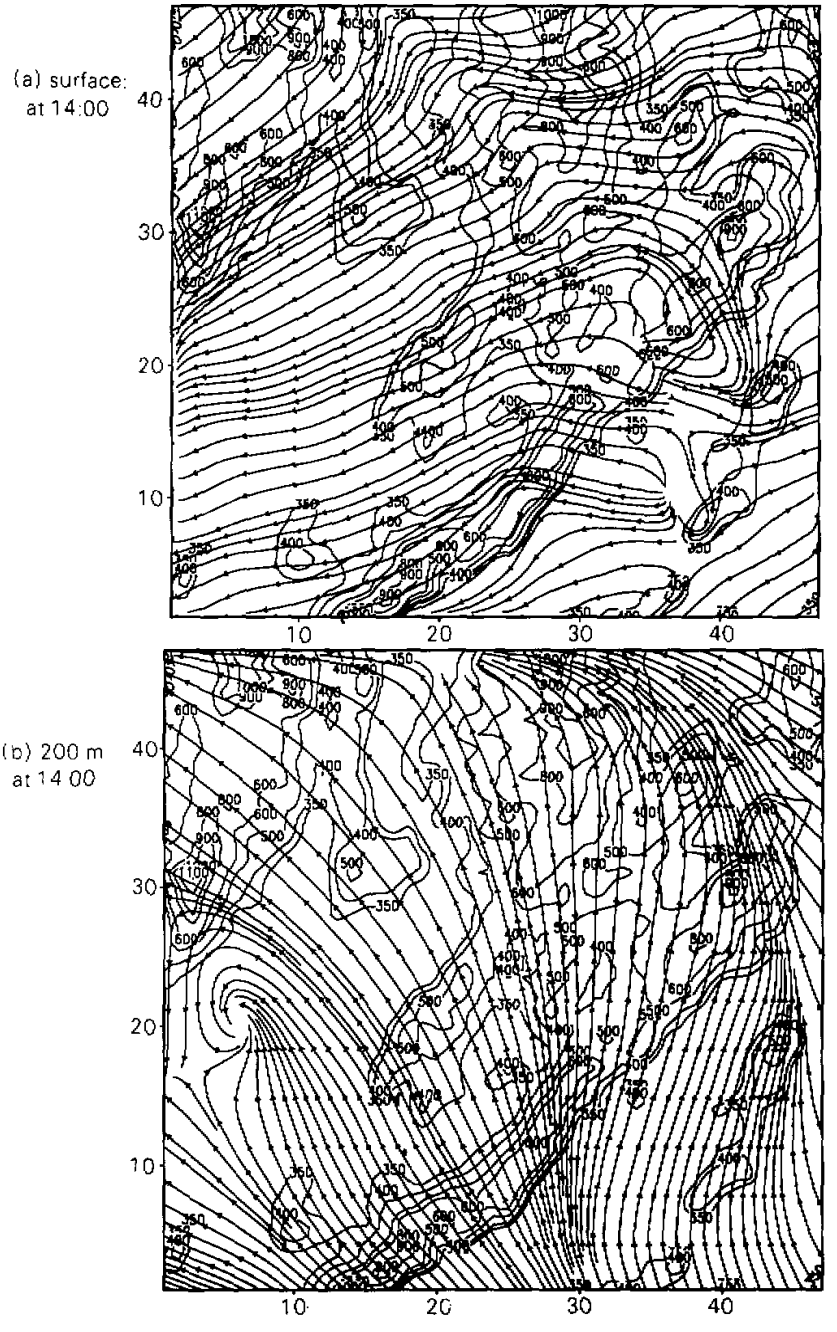

Fig. 1. Wind field simulated by the MM on March 27, 1996.

for every 3 and 6 hours a day, respectively. The height range measured with the Doppler sodar is from 83 to 1000 m and vertical profiles of both wind and temperature are provided for every 20 minutes a day.

The model requires emission rates of SO_2, NO_2, NO. Two high point sources emitted by the power plant are considered only. The effective emissive plume heights are 227 and 416 m, respectively.

3.3 *Comparisons between observational data and modeling results*

In order to test reliability on the application of the coupling model system to the Mae Moh area which is dominated by mountain and valley breeze, the simulated results have been carefully compared with the monitoring concentration data at the same time. The ratios of measured concentrations to simulated results on 10 monitoring stations for SO_2, NO_2 and NO are given in Table 2.

Table 2. Ratios of measured to simulated concentration

Ratio Range		< 0.1	0.1–0.5	0.5–2	2–10	> 10	Mean
SO_2	%	5.4	8.5	44.9	29.6	11.6	1.63 ± 0.87
NO_2	%	0.4	5.0	52.9	40.4	1.3	1.75 ± 0.75
NO	%	0.3	7.4	54.8	34.6	2.9	1.63 ± 0.77

Several results are noted from Table 2. First, the mean ratios of observational concentration data to the simulated values are over than 1.0; one reason is that only two large pollutant sources are considered in the model, and another is that the simulated results represent an average value in an area of 4.0 km^2, but the measured results are valuable only at a fixed point. Second, the average ratio ranging from 1.63 to 1.75 shows that the simulated results are in good agreement with measured data. Third, although standard deviations are largish, all of them are less than the mean ratio. Forth, the frequency distributions in the ratio ranging from 0.5 to 2.0 are 54.8%, 52.9% and 44.9% for NO, NO_2 and SO_2, respectively; the results show that simulated effect of NO is the best in the three species. Fifth, under the complex terrain of the Mae Moh area, the coupling model system can be useful for studies of both regional air quality and environmental assessment.

4. Practical simulated results

4.1 *Distribution laws of flow pattern*

The 3–D wind fields for 6 cases were simulated by the MM. The results on March 27, 1996 are shown in Fig. 1 and Fig. 2.

Several results are noted from wind fields in Fig. 1 and Fig. 2a. First, there are four local convergence and divergence areas near the mountain and valley, there is obvious inhomogeneity of flow pattern in Fig. 1a. Second, horizontal inhomogeneity of surface flow field is due to dynamic and thermodynamic forcing at the surface, the small–scale local forcing can be simulated well by the MM. Third, with increase of height the flow pattern becomes smoother, the effect of the surface forcing becomes weak. Fourth, there are two convergence and divergence areas only at 400 m (Fig. 1b), the depth of effect on the surface forcing is higher than 400 m in the Mae Moh area. Fifth, the flow pattern is very homogeneous at 800 m (Fig. 2a), and the systematic southwest flow dominates all the model area.

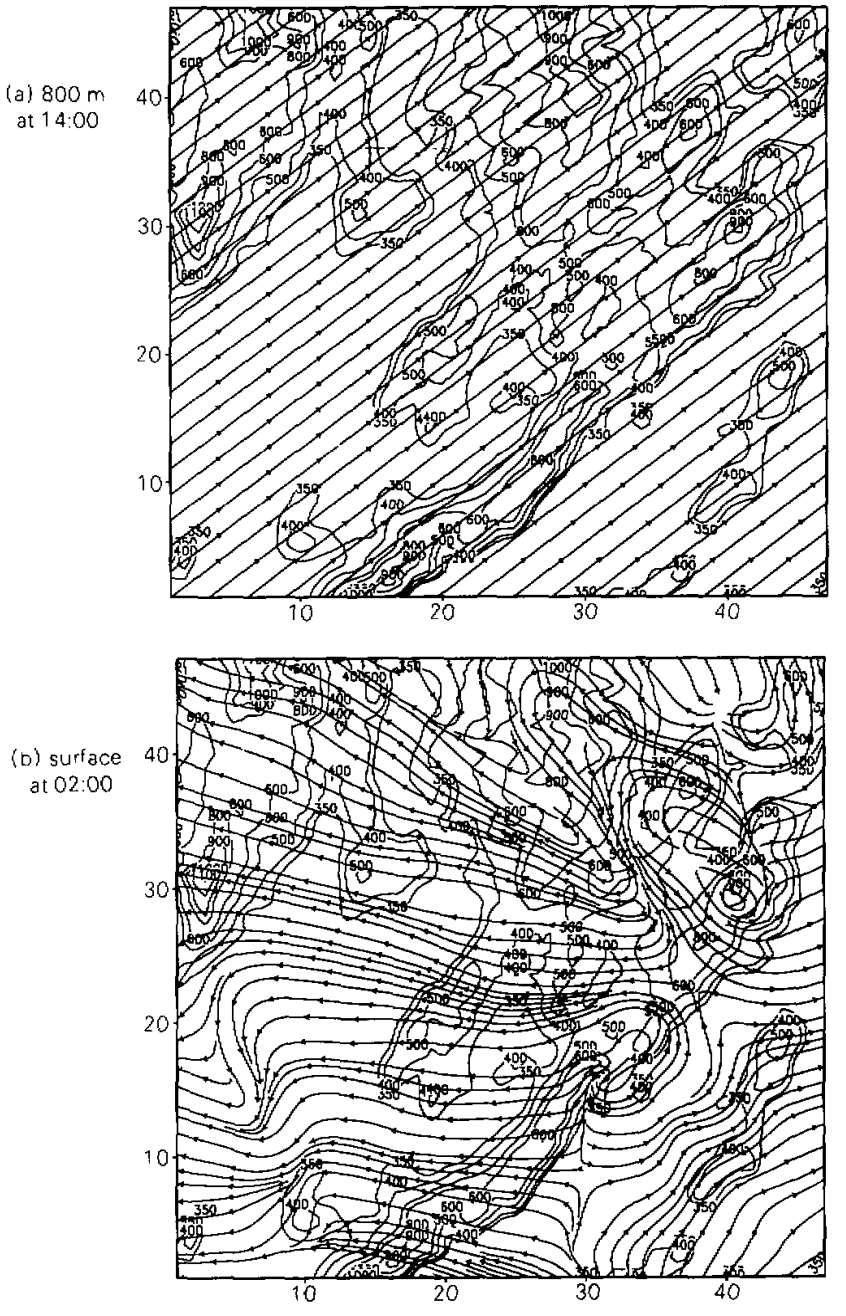

Fig. 2. Wind field simulated by the MM on March 27, 1996.

Because there exist mountain and valley in the model area, local mesoscale circulation formed by different surface heat possesses obvious diurnal variation. Comparison between Fig.2b and Fig.1a shows that the flow fluctuation in the daytime is weaker than that in the nighttime. There are eight local convergence and divergence areas in the model area (Fig. 2b). The results show that scale of the flow fluctuation in the daytime is longer than that in the nighttime. The non–stationary processes due to surface forcing can be simulated well by the MM.

4.2 *Distribution laws of species*

4.2.1 *Distribution laws of* NO_2

Production of NO_2 in the chemical reactions can be described as

$$P_{NO_2} = K_{h4}[HNO_3] + K_5[O_3][NO] + 2K_9[NO][NO][O_2] + 2K_{12}[NO][NO_3] + K_{13}[NO_3][NO_2] + K_8[HO_2][NO]. \quad (21)$$

Loss term in the chemical reactions is given as

$$L_{NO_2} = K_{h1} + K_1[O^3P] + K_{11}[O_3] + K_{13}[NO_3] + K_{15}[HO], \quad (22)$$

where K_i and K_{hi} are the constants of chemical reaction rates for different species, [ ] is the gaseous species concentration.

From expressions (21) and (22) we can see that production and loss of NO_2 are very complex. Several results are noted from concentration fields in Fig. 3. First, the area enveloped by 0.01 $\mu g / m^3$ isoline is larger in the daytime than that in the nighttime; there are two and six centers enveloped by 5 $\mu g / m^3$ isoline in the daytime and nighttime, respectively. Second, these phenomena clearly show that the diurnal variation process, and NO_2 loss due to the photochemical reaction are very considerable. Third, the region which contains six centers enveloped by 5 $\mu g / m^3$ isoline is very large, and the farthest center is about 30 km from source point; these results show that now polluted range in the Mae Moh area has enlarged from a single factory to a vast area, which has become a problem of regional air pollution. Fourth, owing to less primary pollutant NO_x emitted by the Power Plant the NO_2 concentration is less than 15 $\mu g / m^3$.

4.2.2 *Distribution rules of* O_3

O_3 is one of the most important secondary pollutants and it is also an important oxidant and greenhouse gas. O_3 can cause obvious regional pollution. There is complex nonlinear chemical relationship between O_3 and its precursors, such as NO_2, NO.

Production of O_3 in chemical reactions of this study can be described as

$$P_{O_3} = K_{s1}[O^3p][O_2]. \quad (23)$$

Loss term is given as

$$L_{O_3} = K_{h2} + K_{h3} + K_5[NO] + K_6[HO] + K_7[HO_2] + K_{11}[NO_2]. \quad (24)$$

From expressions (23) and (24) we can see that not only NO_x does not produce O_3, but also it loses O_3. In order to analyze formative mechanism of O_3, production and loss terms of O^3p in the chemical reactions are given as,

$$P_{O^3P} = K_{h1}[NO_2] + K_{h3}[O_3] + K_2[O^1D][N_2] + K_3[O^1D][O_2], \quad (25)$$

$$L_{O^3P} = K_1[NO_2] + K_{s1}[O_2], \quad (26)$$

respectively, where K_1, K_{s1} and K_{h1} are the constants of chemical reaction rates for different species. From expressions (22), (23), (24), (25), and (26) we can obtain that the production of O_3 in the troposphere is a very complex process. Although NO_x is not directly related to the production of O_3, close relationship between NO_x and O_3 can be established by P_{O^3P}).

Several results are noted from expressions (22)–(26) and concentration fields in Fig. 3 and Fig. 4. First, the variation of surface O_3 ranges from 0.01 to 50 $\mu g / m^3$ due to chemical processes; the concentration in the daytime is much higher than that in the nighttime. Second, the diurnal variation of concentrations appears obviously, the results show that the production of O_3 in the near surface layer has close relation to the photochemical reaction. Third, the area enveloped by 0.01 $\mu g / m^3$ isoline in the daytime is larger than that in the nighttime, the result shows that the horizontal turbulent diffusion and transport in the daytime are more than those in the nighttime. Fourth, the horizontal inhomogeneity of O_3 concentration distribution is much less than that of NO_2. Fifth, the maximum concentration centers of O_3 correspond approximately to that of NO_2, but they do not completely coincide. Sixth, O_3 concentration in the daytime is much higher than that of NO_2, NO_2 concentration in the nighttime is higher than that of O_3; one reason is that the source strength of primary pollutant NO_2 emitted by the Power Plant is less, and another is that O_3 is a secondary pollutant produced by the photochemical reactions among NO_2, NO and sunlight.

5. Summary and conclusions

After the Lagrangian MCM couples with ENCM, the model system can treat nonlinear chemical processes of species, such as NO, NO_2, O_3 and others.

Parameterized model on variations of the turbulent statistics in the PBL with height, z_0 and atmospheric stability are directly coupled with the MCM.

3–D meteorological fields input into the MCM are directly created by the MM adopting advanced techniques of both FDDA and nested grid.

A NDDVP is used in the MCM, it can better represent effects of different biological landuses and atmospheric stability on dry deposition processes.

A new Lagrangian–Eulerian coupling model system has been developed to study regional air quality. Physical, chemical, and biological processes on air pollutants have been considered comprehensively in the model system. 3–D distribution laws for acidic gaseous pollutants (SO_2 and NO_x) emitted by the Thai Mae Moh Power Plant and the secondary pollutants are studied in detail. The results simulated by the coupling model system are in good agreement with measured concentration data.

The authors wish to express their thanks to Prof. Zeng Q. C. for his support to this research and to Dr. Han Z. W. and Zhang M. G. for their help in programming and numerical calculation of IAP, Chinese Academy of Sciences. Thanks are also due to NSTD and EGAT in Thailand for supporting this research.

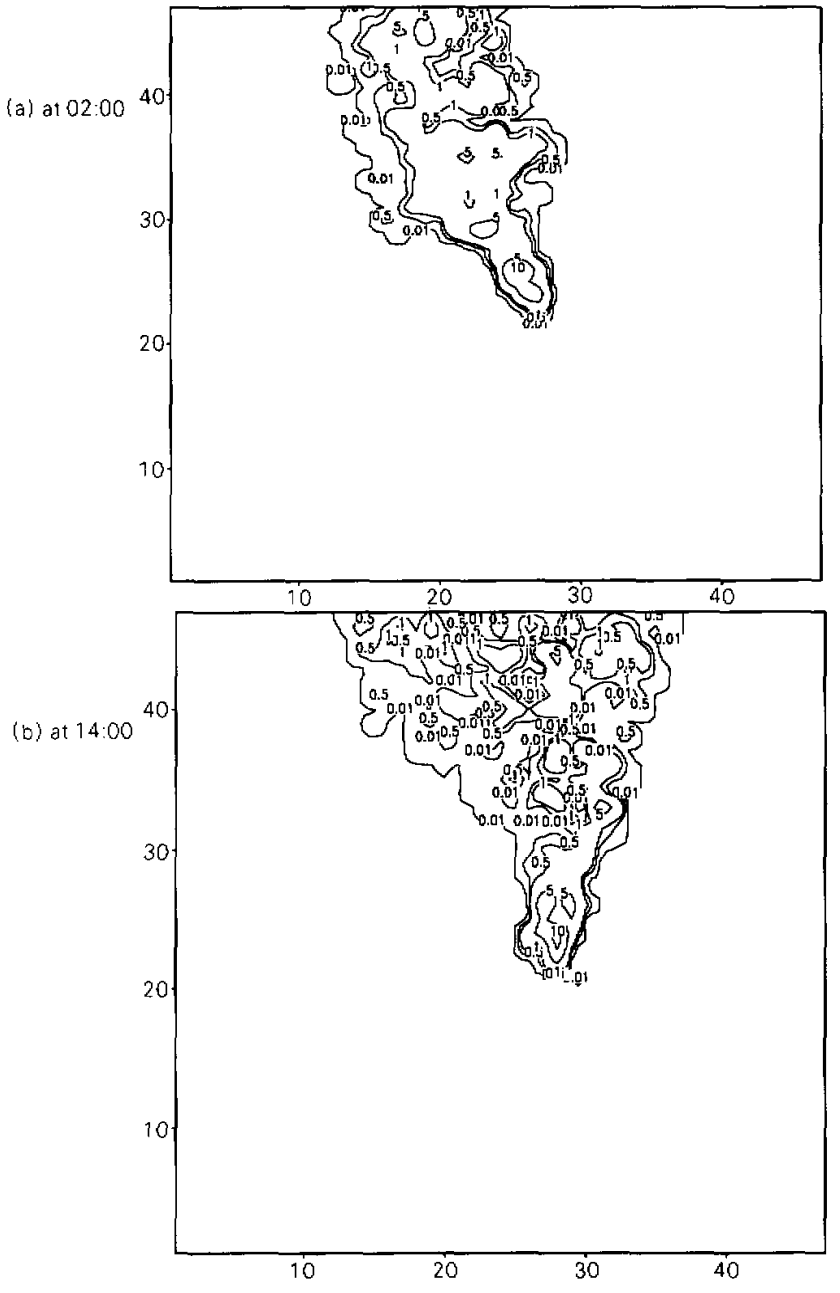

Fig. 3. NO_2 concentration $\mu g / m^3$ simulated by the model system on February 19, 1996.

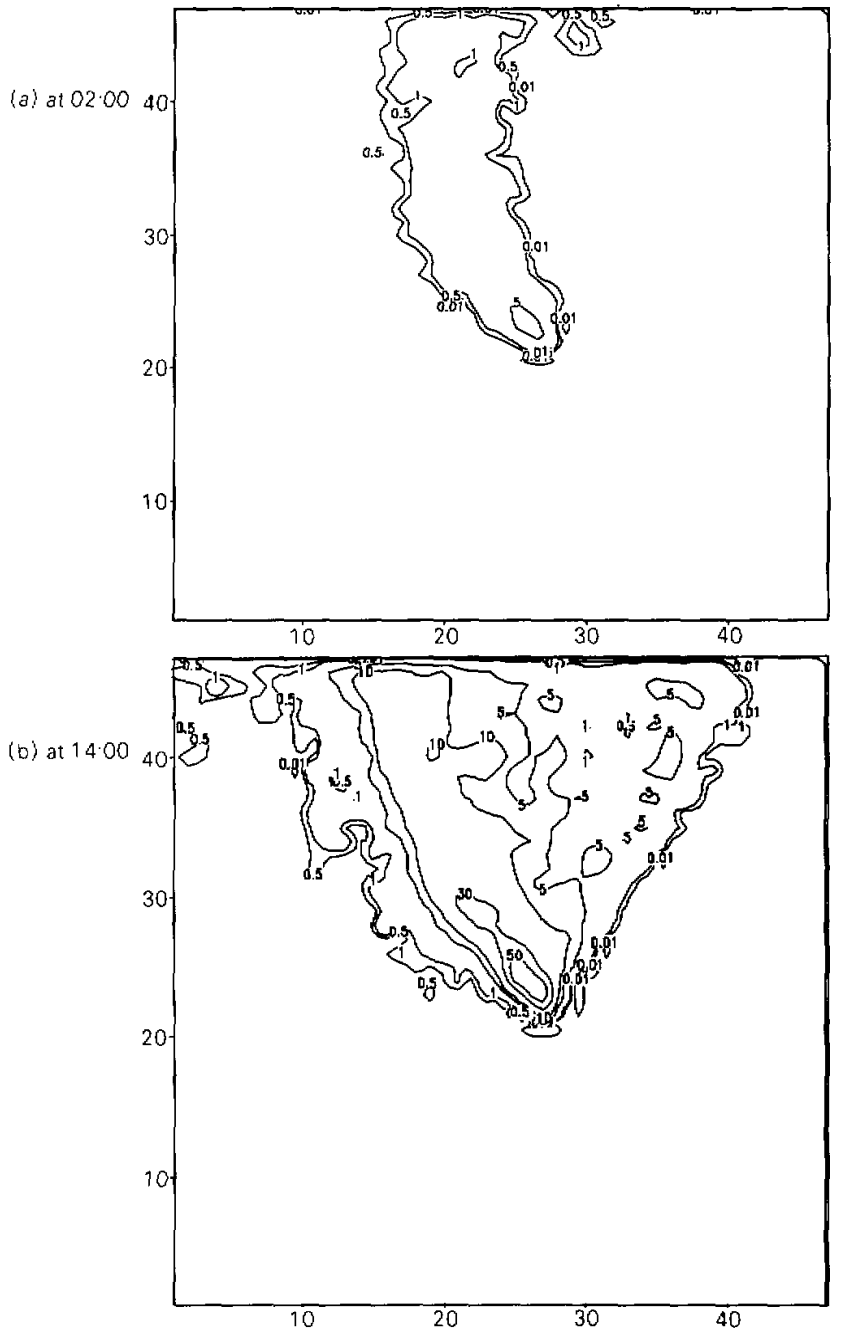

Fig. 4. O_3 concentration $\mu g / m^3$ simulated by the model system on February 19, 1996.

REFERENCES

Anthe, R.A., 1987: Description of the Penn State / NCAR mesoscale model version4 (MM4). NCAR / TN-282+STR, NCAR, 1-66.

Dudhia, J., 1996: PSU / NCAR Mesoscale modeling system tutorial class notes, Mesoscale and microscale meteorology division, NCAR, 66.

Guo, Y. R., 1994: Terrain and land use for the fifth-Generation PS / NCAR mesoscale modeling system (MM5). NCAR / TN-334+IA, 109.

Hanna, S. R., 1979: A statistical diffusion model for use with variable wind fields. *Fourth Symposium on Turbulence, Diffusion, and Air pollution*, AMS, 15-18.

Lei, X. E., Jia X. Y., and Yuan S. Z., 1987: A numerical simulation of the distribution of acid precipitation in Chongqing area in China. *Advances in Atmospheric Sciences*, **4**, 313-322.

Lei, X. E., and Deng Y. Z., 1988: Application of Monte-Carlo method to study of diffusion characteristics and concentration distribution in the mesoscale range. *Annual Report*, IAP, **7**, 232-238.

Lei, X. E., 1988: Parameterization of variable of turbulent statistics and wind speed with height in PBL. *Annual Report*, IAP, **7**, 248-253.

Lei, X. E., and J. S. Chang, 1992: A high resolution model for chemical species exchange in troposphere. *Acta Meteorologica Sinica*, **6**, 479-490.

Lei, X. E., 1996: A new dry deposition velocity pattern and its practical application in high resolution regional acid deposition model. *Acta Meteorologica Sinica*, **10(1)**, 118-128.

Lei, X. E., Han Z. W., and Zhang M.G., 1998: *Physical, Chemical, Biological Processes and Mathematical Model on Air Pollution*. China Meteorological Press, Beijing, 1-355.

McQueen, J. T., 1996: An overview of RAMS as applied at NOAA / ARL. NOAA Technical memorandum ERL ARL., 49.

NAPAP, 1990: The regional acid deposition model and engineering model. Acid deposition: State of science and technology, Report 4.

Scott, B. C., 1982: Theoretical estimates of the scavenging coefficient for soluble aerosol particles as a function of precipitation type, rate and altitude. *Atmospheric Environment*, **16**, 1753-1762.

Seaman, N. L., 1989: Development of FDDA for regional dynamic modeling study. Final report. CR-813068-01-0, EPA, RTP., NC., 102.

Stauffer, D. R., 1990: Use of FDDA in a limited-area mesoscale model. Part I: Experiments with synoptic-scale Data. *Mon. Wea. Rev.*, **118**, 1250-1277.

Stull, R. B., 1988: *An Introduction Boundary Layer Meteorology*. Atmospheric Sciences Library, 649pp.

Walko, R. L., 1995: RAMS, Version 3b, User's Guide, Aster division, Mission research corporation, Fort Collins, CO 850522, 121.